Silver and potassium ion-exchanged waveguides in glasses doped with PbS semiconductor quantum dots

Jason M. Auxier, Seppo Honkanen, Axel Schülzgen, Michael M. Morrell, and Matthew A. Leigh

College of Optical Sciences, University of Arizona, Tucson, Arizona 87521-0094

Sabyasachi Sen and Nicholas F. Borrelli

Glass Research Group, Corning, Inc., Research and Development Center, Sullivan Park, Corning, New York 14831

Nasser Peyghambarian

College of Optical Sciences, University of Arizona, Tucson, Arizona 87521-0094

Received September 23, 2005; accepted December 13, 2005; posted January 25, 2006 (Doc. ID 64949)

We present a detailed analysis of potassium–sodium and silver–sodium ion-exchange processes for fabricating waveguides in glass doped with PbS semiconductor quantum dots. We compare the propagation losses of these waveguides, and we discuss the sources of these losses. In addition, we demonstrate a fourfold reduction in the propagation loss previously reported for potassium–sodium ion-exchanged waveguides and show that waveguides can be produced at additional quantum-dot resonances using both methods. We show that the near-infrared optical properties of these quantum dots remain intact by comparing the waveguide and bulk (unguided) luminescence spectra. Measurements of the near-field mode profiles show a high level of field confinement, which make these waveguides ideal for nonlinear optical (high-intensity) applications.

OCIS codes: 130.3060, 130.3130, 130.5990, 160.3130, 230.7380, 250.5230, 300.6470.

1. INTRODUCTION

Recently, we presented two techniques for manufacturing low-loss waveguides in a glass doped with PbS quantum dots (QDs).[1,2] These previous articles serve as an initial demonstration of the fabrication of low-loss ion-exchanged waveguides in QD-doped glass. In this article we provide a detailed analysis of these ion-exchanged waveguides.

For about a decade, high-quality (narrow-size distribution, $\Delta R/R \approx 5\%$, and few defects) QD-doped glasses have been produced by using the proper thermal treatment of a glass containing the semiconductor's chemical constituents, which precipitates into semiconductor QDs.[3] The three-dimensional quantum confinement of the semiconductor QDs allows tailoring of the optical absorption.[4] The major advantage of semiconductor-doped glasses over epitaxially grown structures is cost. These semiconductor-doped glasses are far less expensive than heterostructures grown through molecular beam epitaxy. Additionally, with the same chemical constituents, QD-doped glass can be produced with a much wider range of absorption coefficients (nearly 3 orders of magnitude) and a wider range of optical resonances (for PbS, from 800 to 2500 nm). These properties make QD-doped glass an attractive candidate for the production of nonlinear optical devices.

The PbS QDs provide strong confinement, since they have radii (2–5 nm) that are smaller than the bulk exciton Bohr radius (18 nm). The small bulk bandgap energy (0.4 eV at 300 K) allows tuning of their optical resonances throughout the near infrared. The room-temperature absorption spectra of several PbS QD-doped glasses (three of which were used to produce waveguides) are shown in Fig. 1. The QD radii R quoted in Fig. 1 are calculated using a hyperbolic band model[5,6]:

$$(\hbar\omega_{1s})^2 = \left(\frac{hc}{\lambda_{1s}}\right)^2 = E_g^2 + \frac{2\hbar^2 E_g}{m^*}\left(\frac{\pi}{R}\right)^2, \tag{1}$$

where we used the room-temperature ($T = 300$ K) bandgap energy of $E_g = 0.41$ eV and effective mass of $m^* = 0.12m_0$ for PbS.[6]

Strongly confined QDs exhibit strong optical nonlinearities,[7] which include bleaching and optical gain. Both of these effects have been measured in these PbS QD-doped glasses.[8–10] These measurements were performed in bulk glasses, whereas most applications are in the areas of fiber and integrated optics.

Because of the semiconductor dopants, drawing a glass fiber that is doped with QDs is difficult. In fact, all attempts have failed owing to the fact that the perform melt must be brought to nearly 1200°C, which is above the melting point of PbS. Additionally, the PbS is produced in the glass with a heat treatment in the range of 600°C–700°C, so the QDs would grow during the fiber-

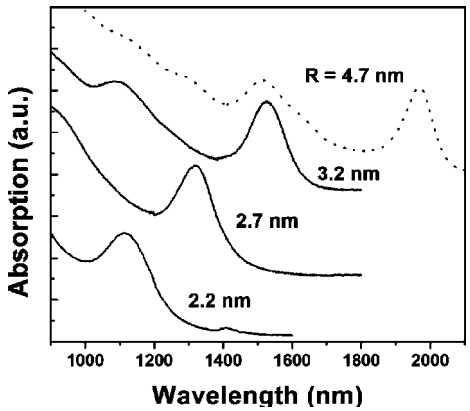

Fig. 1. Room-temperature absorption spectra of PbS QD-doped glasses. Solid curves, samples we used to produce waveguides. The mean QD radii R (calculated using the hyperbolic band model) for each sample is listed.

drawing process.[3] This difficulty of producing fiber with this QD-doped glass has lead us to the fabrication of planar (channel) waveguides in this glass.

Waveguide fabrication in semiconductor-doped glasses is advantageous in order to use the field confinement to enhance the nonlinear interaction by increasing the intensity and the interaction length. The fabrication technique chosen was ion exchange, since it produces a subtle and local change in glass chemistry that alters the index of refraction. This technique is fairly gentle and utilizes lower temperatures (less than 400°C). Waveguides in semiconductor-doped glasses have been reported using K^+-Na^+ ion exchange.[11,12] Recently, we reported measurements of the propagation loss of waveguides in PbS QD-doped glass using K^+-Na^+ and Ag-film ion-exchange processes.[1,2] Here, we report a refinement of the K^+-Na^+ technique that resulted in a fourfold reduction of the propagation loss. Additionally, we have extended both of these techniques to fabricate waveguides in glasses with a variety of resonance wavelengths.

2. WAVEGUIDE FABRICATION

In molten-salt ion exchange, the molten salt supplies replacement ions (usually K^+ or Ag^+ for sodium ions in the glass. The physical mechanism for the ion-exchange process is thermal diffusion of ions to produce a change in the local glass chemistry and thus a change in refractive index. As derived from Fick's first and second laws, the diffusion of silver ions in the glass (Ag^+-Na^+ ion exchange) is given by[13–15]

$$\frac{\partial C_{\mathrm{Ag}}}{\partial t} = \frac{D_{\mathrm{Ag}}}{1-(1-M)C_{\mathrm{Ag}}}\left[\nabla^2 C_{\mathrm{Ag}} + \frac{(1-M)(\nabla C_{\mathrm{Ag}})^2}{1-(1-M)C_{\mathrm{Ag}}} - \frac{q\mathbf{E}_{\mathrm{ext}}\cdot\nabla C_{\mathrm{Ag}}}{kT}\right]. \quad (2)$$

Here, D_{Ag} and D_{Na} are the self-diffusion coefficients of silver and sodium, respectively, and $M=D_{\mathrm{Ag}}/D_{\mathrm{Na}}$ is their ratio. C_{Ag} and C_{Na} are the concentrations of silver and sodium in the glass, respectively; however, it is customary to normalize these concentrations so that $C_{\mathrm{Na}}=1$. Since this article does not focus on modeling, we refer the reader to the work of West *et al.*[13] Tervonen,[14] and Albert and Lit[15] for the proper boundary conditions and their application. We point out that, for the case of $M=1$, this equation reduces to the familiar diffusion equation. Also notice that, for a salt-melt ion exchange (no external field), the first two terms in square brackets dominate. For an Ag-film ion exchange, the last term in square brackets dominates.

The ion-exchange produces an index change by altering the local glass density and mean polarizability.[16,17] The Lorentz–Lorenz formula describes the polarizability.[16] The refractive index change is linear (ignoring mechanical stress) with the normalized silver concentration C_{Ag}:

$$n(x,y,\lambda) = n_{\mathrm{sub}}(\lambda) + \Delta n_{\max}(\lambda) C_{\mathrm{Ag}}(x,y), \quad (3)$$

where n_{sub} is the substrate index before ion exchange and $\Delta n_{\max}(\lambda)$ is the increase in refractive index (at optical wavelength λ) resulting from a complete replacement of silver for sodium in the glass, i.e., $C_{\mathrm{Ag}}=1$. This analysis can be used for K^+-Na^+ ion exchange when we replace C_{Ag} and D_{Ag} in Eqs. (2) and (3) with C_{K} and D_{K}, respectively. However, the analysis is only indicative, since the stress-induced index change is significant in K^+-Na^+ ion-exchanged waveguides.

The Ag^+-Na^+ ion-exchange process is used to produce commercially available planar lightwave circuits[17] (PLCs). These PLCs are fabricated using a field-assisted burial process that results in waveguides with extremely low loss and birefringence.[17] The work described here is a large step toward the commercialization of QD-doped ion-exchanged waveguides.

A. Potassium–Sodium Ion-Exchange Process

In the potassium–sodium ion-exchange process, a potassium nitrate molten salt supplies potassium replacement ions for sodium ions in the glass. Some of the lowest reported propagation losses for ion-exchanged waveguides have been obtained using K^+-Na^+ ion exchange. The downfall of K^+-Na^+ ion-exchanged waveguides is the diffusion coefficient and lower index change, which prevent these waveguides from being buried.

To get an estimate of proper exchange times for a particular temperature, we performed several exchanges to produce slab waveguides in this glass. Using a prism coupler, we measured the effective indices (at 633 nm) of the slab modes produced from a long exchange (405 h at 380°C in pure KNO_3). The maximum index change was estimated to be $\Delta n_{\max}\approx 0.012$ at 633 nm by using Chiang's inverse Wentzel–Kramers–Brillouin (WKB) method.[18] This showed that K^+-Na^+ ion exchange results in a large enough index change to produce channel waveguides. Also, using this analysis on shorter exchanges (one, seven, and ten days), we were able to estimate an appropriate exchange time for the fabrication of single-mode channel waveguides in this glass.

Figure 2 is a diagram of the ion-exchange process. In preparation for the ion-exchange process, the glass sample was surface polished. Our glass is experimental and comes straight from a glass pour. Therefore, we lapped the 50 mm (diameter) glass wafer flat ($\sim\lambda/2$ at 1550 nm) by using a 9 μm followed by a 3 μm aluminum oxide slurry on a cast-iron plate. The wafer was polished

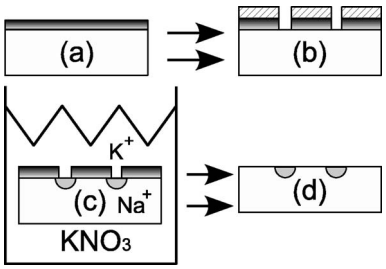

Fig. 2. Potassium–sodium ion-exchange process. After surface polishing and cleaning, (a) the glass is coated with titanium; (b) the glass is coated with photoresist, patterned, and cured, and the titanium is etched (photolithography process); (c) the glass is placed into a KNO_3 molten salt; and (d) the titanium ion-exchange mask is removed for sample characterization. (c) The K^+–Na^+ ion exchange, where potassium ions in the salt replace sodium ions in the glass. This local change of glass chemistry produces the waveguides.

using two polishing steps on a polyurethane polishing plate. For the first step, we used 1 μm aluminum oxide, and, for the fine polishing, we used 0.3 μm aluminum oxide. Cerium oxide could not be used, since it chemically reacted with the sulfur in the QD-doped glass (producing deep pits). After polishing, we inspected the polish using a microscope with 200× compound magnification to ensure an optical-quality polish. We polished both sides of each wafer and used the better side for the lithography. After cleaning, this optical-quality polish allowed us to produce a high-quality film of titanium as depicted in Fig. 2(a). Note that we cannot overemphasize the importance of having high-quality polishing and titanium films, since surface scattering is the predominate loss mechanism.

Figure 2(b) shows the lithographic step for the ion-exchange process. After each step of the lithographic process, the wafer is inspected with a high-magnification microscope to ensure quality. Here, we coat the titanium with photoresist, which was patterned, developed, and cured (30 min at 120°C). The patterning of the photoresist uses a standard lithography procedure with a chromium mask. The developed photoresist serves as a mask for titanium etching. The titanium is etched using an acid solution (0.6 g ethylenediamine tetra-acetic acid, 30 ml deionized H_2O, and 15 ml H_2O_2) at 60°C for about 20 s. Care must be taken not to underetch or overetch the titanium. We often intentionally slightly underetched the titanium so we could inspect the etching process under the microscope. Once we were satisfied with the level of etching, we removed the photoresist using acetone.

After cleaning, the sample is now ready for the ion exchange. Figure 2(c) depicts the ion-exchange process. Here, the exchange of ions occurs in a KNO_3 salt melt. Potassium ions in the salt exchange with sodium ions in the glass, producing a local chemical change along with a corresponding index change. For our QD-doped glass, we used pure KNO_3 molten salt at 370°C for 200–260 h. To reduce thermal shock, we placed the samples into a separate oven for 20 min before and after ion exchange. After cooling, the sample was rinsed, and the titanium was removed [Fig. 2(d)] by using a doubled-concentration acid solution. At this point, the sample can be processed for device characterization.

To do this, we cleaned, cut, and polished the sample. Since the waveguides are surface waveguides (about 10 μm wide), creating a square edge with few chips is important. To do this, we stack several samples (waveguide surfaces facing each other) into an edge-polishing jig. For well-polished surfaces and minimal surface damage due to the ion-exchange and etching processes, van der Waals force will draw the glasses close together, resulting in widely spaced Newton's interference fringes. We start the polishing process by lapping the edges with a 3 μm aluminum oxide slurry on a cast-iron plate so that the edges are even. After lapping, the glass is inspected to ensure quality. For satisfactory results, the edge of the glass stack should look like one solid piece of ground glass, that is, the lines separating the individual pieces of glass should disappear. Then we polish the edge on a soft, polyurethane polishing pad by using 1 μm aluminum oxide for a rough polish and 0.3 μm aluminum oxide for the final polish. The glass is again inspected to ensure quality. After cleaning, the samples are ready for device characterization.

B. Silver-Film Ion-Exchange Process

The most common ion-exchange process is Ag^+–Na^+ ion exchange using a silver nitrate salt melt. Even though this process has produced low-loss waveguides in silicate and phosphate glasses, there has not been any report of using this process to produce waveguides in any semiconductor-doped glass, to our knowledge. Here, we overcame the problem of silver reduction by using an Ag-film process[19,20] instead of a salt-melt process.

From an application standpoint, Ag^+–Na^+ ion exchange produces a higher index change than K^+–Na^+ ion exchange. Using a prism coupler to measure the effective indices of slab modes, we estimated a maximum index change of $\Delta n_{max} \approx 0.045$ at 633 nm by using the inverse WKB method.[18] This gives Ag^+–Na^+ ion exchange a major advantage, since it allows for smaller mode sizes, higher field confinement, and the waveguides to be buried. Burial and annealing of the waveguides minimize surface interaction, coupling loss, and birefringence.[21]

As depicted in Fig. 3, Ag-film ion exchange involves an applied electric field to drive silver replacement ions from a thin film of silver into the glass. Here, sodium ions are driven further into the thickness of the glass. This applied electric field keeps the ions moving in the glass, which prevents silver nanocrystal formation (by means of reduction). Ag-film ion exchange has been used to produce waveguides in undoped glass[19,22] and in Er-doped glass[23]; however, until our recent report,[2] semiconductor-doped

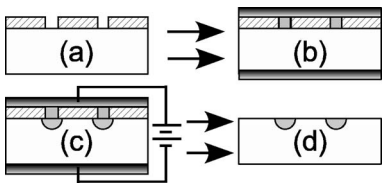

Fig. 3. Ag-film ion-exchange process. After surface polishing and cleaning, the glass is (a) coated with photoresist, patterned, cured, and (b) coated with silver on both sides; (c) a dc field is applied for ion exchange; and (d) the silver is stripped off, and the glass is annealed. For our ion exchange, we used a field of 250 V/mm at 110°C and annealed the glass for 2.5 h at 200°C.

waveguides have never been reported using any type of Ag^+-Na^+ ion exchange, to our knowledge.

Figure 3 depicts the Ag-film ion-exchange process. In this process the ion-exchange mask consists of patterned photoresist.[24] This photoresist eliminates adhesion of the silver film on the glass in locations where we do not want waveguides. With the method described in Subsection 2.A, the glass sample is carefully surface polished and cleaned. As shown in Fig. 3(a), the clean, polished sample is coated with photoresist, developed, and cured (30 min at 150°C). The developed photoresist serves as the ion-exchange mask, which can contain any two-dimensional pattern to form any PLC. As shown in Fig. 3(b), the photoresist and the back surface of the glass is coated with a thin (100–150 nm) film of silver.

Figure 3(c) shows the actual ion exchange, which occurs in an oven set to around 100°C. The ion exchange is performed by application of a dc electric field (typically, a few hundred volts per millimeter, producing a few microamperes of current), which drives silver ions into the glass. For this glass, single-mode waveguides were produced by using the following exchange parameters: 4.5 h, 110°C, and 250 V/mm. In this ion-exchange process, the dc field drives silver ions into the glass. Only a shallow region in the glass has a significant concentration of silver ions. Figure 3(d) shows the removal of the residual silver. The sample is then cut and polished for device characterization by using the techniques described in Subsection 2.A. Then the glass is annealed (2.5 h at 200°C) to allow the silver to diffuse further into the glass, making the index profile smoother.

3. WAVEGUIDE CHARACTERIZATION

A. Refractive Index and Optical Mode Profiles

To compare the waveguides fabricated using these two ion-exchange techniques, we measured index profiles by using the refracted near-field (RNF) technique.[1,25,26] As described by Göring and Rothhardt,[25] we used a modified microscope to infer the critical angle for total internal reflection (TIR). Applying Snell's law to each interface while tracing the meridional ray through the RNF system, we can solve for the refractive index $n(x,y)$ at the focused spot of the waveguide[26]:

$$n^2(x,y) = \sin^2\theta_{\text{in}} + n_{\text{ref}}^2 + \sin^2\theta_{\text{out}}, \tag{4}$$

where n_{ref} is the index of refraction of the reference block and θ_{in} and θ_{out} are incident and exit angles, respectively. Since the reference block is made of BK7 glass, n_{ref} is known. The index profile is built up by one's scanning the focused spot over the front face of the sample. Now, owing to TIR, there will be a maximum input angle, θ_{in}, where light is transmitted through the optical system to the large-area detector. Therefore, assuming that the index variations are small, the power incident on the detector is proportional to the refractive index profile (with a dc offset).[26]

In addition, we measured the near-field mode profiles of several channel waveguides. To do this, we coupled 1550 nm light into a waveguide and imaged the output mode onto a near-infrared camera using a 0.6 NA objective. These modes were also used to calculate ideal coupling losses between the waveguide and the single-mode fiber (Corning SMF-28).

Figure 4 shows the index and mode profiles of typical waveguides using K^+-Na^+ and Ag-film ion exchanges on the left and right, respectively. For the K^+-Na^+ ion-exchanged waveguide measured in Figs. 4(a) and 4(c), we used the following ion-exchange parameters: 370°C for 263 h in a pure KNO_3 salt melt. By adjustment of the coupling conditions, this waveguide was found to have a second mode at 1550 nm. For the Ag-film ion-exchanged

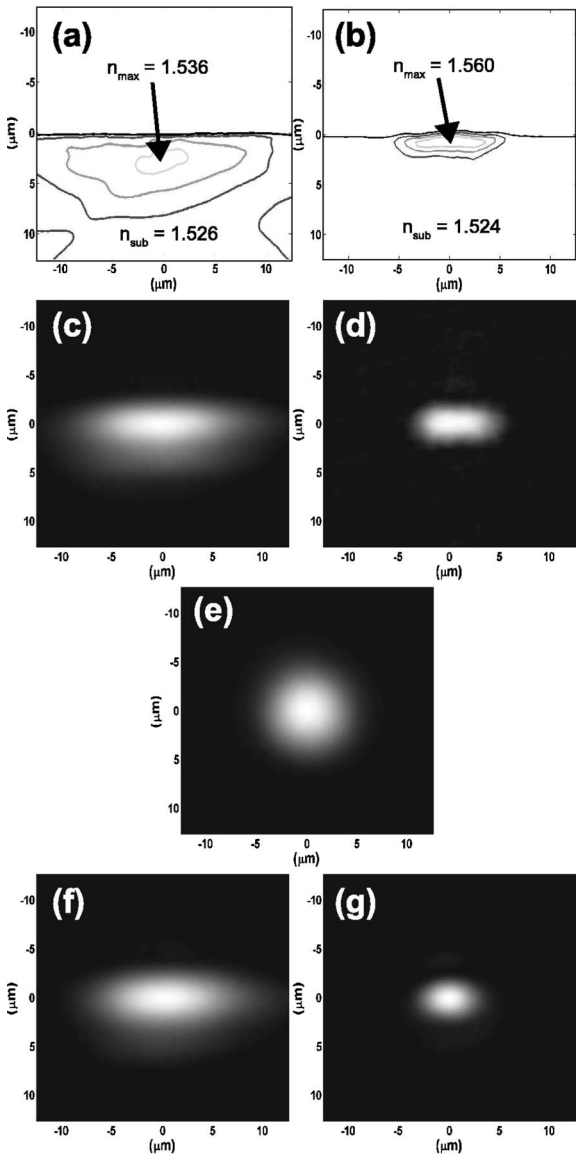

Fig. 4. Optical characterization of QD-doped waveguides fabricated using (left column) K^+-Na^+ and (right column) Ag-film ion exchange. (a) and (b) RNF index profiles (0.8 NA microscope, 633 nm light) from waveguides along with their near-field optical mode profiles (0.6 NA microscope objective, 1550 nm light). For reference, we show the mode profile of (e) SMF-28 along with (f) and (g) single-mode waveguides. The index contours have been smoothed and are separated by (a) $\delta n = 0.0025$ and (b) $\delta n = 0.01$. We measured a 21.4 μm e^{-1} width and a 8.7 μm e^{-1} height for the mode pictured in (f) and a 7.5 μm e^{-1} width at a 5.8 μm e^{-1} height for the mode pictured in (g). The calculated coupling losses (with respect to the SMF-28) are $\gamma = 2.2$ and $\gamma = 1.4$ dB.

waveguide measured in Figs. 4(b) and 4(d), we used the following ion-exchange parameters: 110°C, 18 h, 250 V/mm, followed by a 1.33 h annealing at 200°C. This waveguide was also found to have a second mode. For the single-mode K^+-Na^+ ion-exchanged waveguide measured in Fig. 4(f), we used the following ion-exchange parameters: 370°C for 240 h in a pure KNO_3 salt melt. For the single-mode Ag-film ion-exchanged waveguide measured in Fig. 4(g), we used the following ion-exchange parameters: 110°C, 4.5 h, 250 V/mm, followed by a 2.5 h annealing at 200°C.

Notice that there is a much larger index contrast for the Ag-film waveguide ($\Delta n_{\max}=0.036$) as compared with the index contrast of the K^+-Na^+ waveguide ($\Delta n_{\max}=0.01$). This gives Ag-film waveguides much more flexibility for annealing and burial processes. Also notice that the region of high index change in the Ag-film index profile remains much closer to the surface (about 1 μm) than the region of high index change in the potassium index profile (about 2.5 μm). As shown in the next section, this proximity of the Ag-film mode near the surface increases the surface interaction and thus increases the propagation loss.

Notice that these waveguides are single mode and that the Ag-film waveguides are much smaller than the SMF-28 mode, which is smaller than the potassium waveguide mode. Both of the ideal coupling losses (overlap integral) of these modes with respect to SMF-28 were slightly larger than 1 dB. In either case, these waveguides provide large field confinement, which is good for nonlinear interaction; however, Ag film has the advantage here. The vast difference in maximum index change contributes to the size difference seen in the potassium and silver ion-exchange waveguides. Note that the size of the index and mode profiles could be increased significantly in the Ag-film ion-exchanged waveguides through further annealing, by allowing silver ions to further diffuse in the glass. The diffusion of ions causes significant side diffusion, which allows the waveguides to extend beyond the mask-opening width.

Note that the index profiles were measured at 633 nm and the mode profiles were measured at 1550 nm. The spatial resolution of the RNF microscope used for the index profile is approximately 0.5 μm, whereas the spatial resolution of the optical system used for measuring the mode profile is approximately 1.5 μm. These resolutions are given by the Rayleigh criterion:

$$\Delta d = 1.22\lambda f_{/\#} = \frac{1.22\lambda}{2\mathrm{NA}}. \tag{5}$$

The levels of optical resolution for the index and mode profiles were sufficient to see the features of interest.

B. Waveguide Losses

The losses were analyzed by using the fiber–waveguide–objective method.[1] In this method, we performed a calibration and then four measurements on each waveguide as shown in Fig. 5. For the measurements using a fiber to collect the waveguide output, we used a fiber-coupled photodetector to measure the power. For the measurements using the microscope objective to collect the waveguide output, we used a free-space photodetector to measure the power. The input power was fixed in order to make our calculations easier. The calibration consisted of two power measurements, as depicted by Figs. 5(f-o) and 5(f-f). The first calibration measurement was transmission of the objective P_{fo}, and the second was used to correct any butt-coupling loss between two single-mode fibers P_{ff}. Then we made a transmission measurement with a single-mode fiber (Corning SMF-28) coupled to the input and the output light collected by a high-NA microscope objective (P_{fwo_1}) as shown in Fig. 5(f-w-o_1). Figure 5(f-w-f_1) depicts the next measurement, in which we replaced the output objective with a single-mode fiber (P_{fwf_1}). The last two measurements shown in Figs. 5(f-w-o_2) and 5(f-w-f_2) were repetitions of the previous two measurements with the waveguide flipped around. These measurements are denoted by P_{fwo_2} and P_{fwf_2}, respectively. For powers measured in dBms, we normalized these four waveguide measurements to produce transmission measurements (in dBm) by using

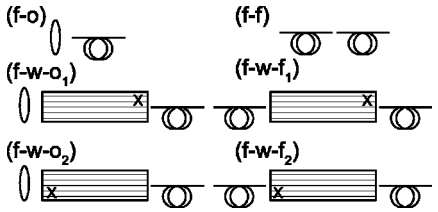

Fig. 5. Fiber–waveguide–objective method for the measurement of losses in optical waveguides. To begin, a calibration is performed. This consists of (f-o) fiber–objective and (f-f) fiber–fiber transmission (power) measurements. The first two waveguide measurements are (f-w-o_1) fiber–waveguide–objective and (f-w-f_1) fiber–waveguide–fiber transmission measurements. (f-w-o_2) and (f-w-f_2) The two transmission measurements in (f-w-f_2) and (f-w-f_1) are repeated with the sample turned around. Measurements (f-w-o_1) and (f-w-o_2) are normalized to measurement (f-o); measurements (f-w-f_1) and (f-w-f_2) are normalized to measurement (f-f). We used Corning SMF-28 fibers and a 0.6 NA microscope objective for these measurements.

$$T_{\mathrm{fwo}_1} = P_{\mathrm{fwo}_1} - P_{\mathrm{fo}}, \tag{6}$$

$$T_{\mathrm{fwo}_2} = P_{\mathrm{fwo}_2} - P_{\mathrm{fo}}, \tag{7}$$

$$T_{\mathrm{fwf}_1} = P_{\mathrm{fwf}_1} - P_{\mathrm{ff}}, \tag{8}$$

$$T_{\mathrm{fwf}_2} = P_{\mathrm{fwf}_2} - P_{\mathrm{ff}}. \tag{9}$$

Now, the losses (in dBm) were inferred by using conservation of energy and are given by

$$L_{\mathrm{side1}} = T_{\mathrm{fwo}_1} - T_{\mathrm{fwf}_1}, \tag{10}$$

$$L_{\mathrm{side2}} = T_{\mathrm{fwo}_2} - T_{\mathrm{fwf}_2}, \tag{11}$$

$$L_{\mathrm{prop}} = T_{\mathrm{fwf}_1} - L_{\mathrm{side2}} = T_{\mathrm{fwf}_2} - L_{\mathrm{side1}}, \tag{12}$$

$$L_{\mathrm{err}} = |T_{\mathrm{fwf}_1} - T_{\mathrm{fwf}_2}|, \tag{13}$$

where L_{side1} and L_{side2} are the two coupling losses, L_{prop} is the propagation loss, and L_{err} is the measurement error. Notice that the losses are defined to be positive, so L = negative decibles $= -10 \log T$, where T is the transmission. As seen in the last equation, an estimate of the measurement error is provided by the redundant fiber–waveguide–fiber measurements. For all of our measurements, we rarely saw an error of larger than 0.2 dB. Note that these losses (in decibels) are logarithmic, so they can be translated to transmissivities through replacing differences by quotients. These losses were measured and calculated for waveguides fabricated using both Ag-film and K^+-Na^+ ion exchange.

In addition, the measured mode profiles were used to calculate the ideal coupling efficiencies of these modes by using[27]

$$\eta = \left| \int_{-\infty}^{+\infty} \int_{-\infty}^{+\infty} \sqrt{I_1(x,y)} \sqrt{I_2(x,y)} \mathrm{d}x\mathrm{d}y \right|^2, \tag{14}$$

where η is the coupling efficiency between the two intensity profiles $I_1(x,y)$ and $I_2(x,y)$ of the two modes. With this coupling efficiency η, the coupling loss is given by $\Gamma = 1 - \eta$. $I_1(x,y)$ and $I_2(x,y)$ are normalized by

$$\int_{-\infty}^{+\infty} \int_{-\infty}^{+\infty} I_i(x,y) \mathrm{d}x\mathrm{d}y = 1, \tag{15}$$

where $i = 1, 2$. When calculating coupling loss in decibels, one simply uses $L = -10 \log \eta$, so if $\eta = 0.5$, then $L = 3$ dB.

Table 1 summarizes the losses of a set of QD-doped waveguides fabricated by Ag-film ion exchange. Table 2 summarizes the losses of a set of QD-doped waveguides fabricated by K^+-Na^+ ion exchange. In these tables, we provide the measured propagation, guide, coupling, and ideal coupling losses. All measurements were performed with 1550 nm light. The ideal coupling losses were calculated using Eq. (14). The guide losses are calculated by our taking the propagation losses and subtracting the bulk QD absorption. To measure the bulk QD absorption

Table 1. Average Propagation, Guide (QD Absorption Removed), Coupling, and Ideal Coupling Losses [Overlap Integral Using Eq. (14)] in QD-Doped Waveguides Made Using Ag-Film Ion Exchange[a]

Mask Width (μm)	Propagation Loss (dB/cm)	Guide Loss (dB/cm)	Coupling Loss (dB)	Ideal Loss (dB)
2	3.5±0.8	2.3	2.4±03	1.6±0.3
3	3.7±0.5	2.5	1.9±0.2	1.4±0.3
4	4.3±0.6	3.2	1.5±0.1	1.4±0.3

[a]All of the these measurements were made at 1550 nm. The ion-exchange parameters were 250 V/mm at 110°C for 4.5 h, followed by annealing at 200°C for 2.5 h. This glass has the absorption spectrum shown in Fig. 1 with QD radius of R = 3.2 nm. The errors quoted for the propagation and coupling losses are standard deviations (five waveguides for each mask width). We estimated the ideal loss error by calculating overlap integrals using various image-processing techniques. We estimate the measurement errors to be 0.5 dB/cm for the propagation losses and 1.0 dB/cm for the guide loss.

Table 2. Average Propagation, Guide (QD Absorption Removed), Coupling, and Ideal Coupling Losses [Overlap Integrals Using Eq. (14)] in QD-Doped Waveguides Made Using K^+-Na^+ Ion Exchange[a]

Mask Width (μm)	Propagation Loss (dB/cm)	Guide Loss (dB/cm)	Coupling Loss (dB)	Ideal Loss (dB)
3	0.4±0.2	0.1	1.5±0.4	1.2±0.5
3.5	0.7±0.5	0.4	1.4±0.4	1.2±0.5
4	0.3±0.1	<0.1	1.3±0.1	1.1±0.5
5	0.2±0.1	<0.1	1.3±0.1	1.0±0.5

[a]All of these measurements were made at 1550 nm. For this ion exchange, we used a pure KNO_3 salt melt at 370°C for 263 h. This glass has the absorption spectrum shown in Fig. 1 with QD radius of R = 2.7 nm. The errors quoted for the propagation and coupling losses are standard deviations (three waveguides for each mask width). We estimated the ideal loss error by calculating overlap integrals using various image-processing techniques. We estimate the measurement errors to be 0.2 dB/cm for the propagation losses and 0.3 dB/cm for the guide loss.

near the waveguide, we placed the sample (lengthwise) in a collimated beam with a beam waist of 400 μm in diameter (Rayleigh range of a few centimeters).

All the errors that are quoted in Tables 1 and 2 are the standard deviations of the waveguide measurements. We also performed a detailed analysis of the measurement errors for the coupling and propagation losses. This included the fiber–waveguide–fiber measurement error [Eq. (13)], a measurement stability error, and a reproducibility error. Adding these errors in quadrature (square root of the sum of the squares), we estimated a 0.5 dB/cm error for the propagation losses shown in Table 1 (Ag-film waveguides) and a 0.2 dB/cm error for the losses shown in Table 2 (K^+-Na^+ waveguides). The measurement errors for the QD-absorption measurements were estimated to be 0.5 and 0.1 dB/cm for these Ag-film and K^+-Na^+ waveguides, respectively.

These waveguides not only provide optical confinement but they also are semihomogeneously doped with PbS QDs. The linear absorption through the thickness of the glass remained unchanged throughout the ion-exchange process. Scattering processes (surface, Rayleigh, and Mie) in the waveguides overshadow the small, linear QD absorption of $\alpha \approx 0.3\ \mathrm{cm}^{-1}$. For a reference, we produced waveguides in the host glass (no QDs) by using both Ag-film and K^+-Na^+ ion exchanges. Within experimental error, guides in the host glass (without QDs) had the same losses as the guides in the QD-doped glass. Additionally, using the 400 μm collimated beam, we found that these host glass samples had as much or more bulk loss owing to scattering as the QD-doped glasses. This suggests that the nonuniformity of the glass and surface interaction is the predominate source of the waveguide losses.

To investigate this surface scattering, we measured the loss as a function of wavelength. To do this, we used an optical spectrum analyzer and a broadband source (1150–1700 nm) in a fiber–waveguide–fiber configuration [see Fig. 5(f-w-f_1)], and we measured the transmission spectra of many waveguides. For a calibration, we measured the broadband source spectrum by using the fiber–fiber configuration shown in Fig. 5(f-f). Note that we inserted the sample and free aligned the input and output

fibers to the waveguide without disconnecting any of the fiber-patch cables. This ensured that we did not change any coupling conditions of the fibers that would lead to multimode interference. The transmission spectrum of the waveguide was normalized to the source-calibration spectrum to find the loss (absorption) spectrum of the waveguide. In measuring the waveguide spectra, we carefully altered the input and output coupling conditions to minimize multimode interference. When necessary, we used index-matching fluid for these fiber–waveguide connections. Once the fibers were aligned to the waveguide, we were able to see the cutoff wavelength (transition between single-mode and multimode operations) of the waveguide. The Ag-film waveguides shown in Table 1 and Fig. 4(g) had a cutoff wavelength of about 1250 nm. The K^+–Na^+ waveguides shown in Table 2 had a cutoff wavelength of about 1300 nm. The host waveguides had a cutoff wavelength of about 1700 nm.

We found that the transmission loss coefficient through the waveguides has a $1/\lambda^x$ ($x=1.3-1.9$) dependence, whereas the Rayleigh scattering of the QDs in the glass has an absorption ($\alpha=\ln T$) with a $1/\lambda^4$ dependence. This wavelength dependence is consistent with reports of surface scattering of slab waveguides using an exponential correlation function.[28–32] The exponent of the wavelength dependence is determined by details such as surface interaction, correlation length, and correlation depth. This analysis suggests that the sample uniformity and surface quality is extremely important for the production of low-loss waveguides.

C. Quantum-Dot Emission

Since scattering predominates waveguide losses, we could not definitively see the structure of the QD absorption in the transmission loss spectra. So, instead of a direct measure of QD absorption in the waveguides, we collected photoluminescence (PL) emitted by the semiconductor QDs within the waveguides. The spectral location and shape of this PL is characteristic of the size and shape of the PbS QDs; therefore, any change in QD chemistry, size, or shape as a result of the waveguide fabrication process would be observed as a change of the PL spectrum.

Figure 6 shows three collection schemes used to collect luminescence from PbS QD-doped waveguides. In all three setups, we coupled the pump light into the waveguide by using a microscope objective. In the first setup, we inserted the entire sample in an integrating sphere and collected the light from a side port. In the second setup, we used a multimode fiber to collect light from the top of the waveguide. In the third setup, we collected the light leaving the exit facet of the waveguide.

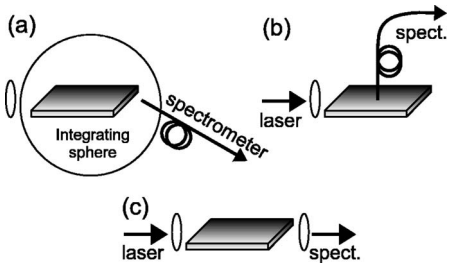

Fig. 6. Three collection setups used to collect luminescence from waveguides in PbS QD-doped glass. These used (a) an integrating sphere, (b) a multimode fiber (100 μm core and a 140 μm cladding), and (c) a 0.45 NA microscope objective. In all three cases, the pump laser beam was coupled into the waveguide by using a 0.45 NA microscope objective, and the collected light was analyzed using a grating spectrometer. In the case of (a), we used the multimode fiber to collect light from an output port of the integrating sphere. In the case of (b), the multimode fiber collected PL emitted from the waveguide coming out the top of the sample.

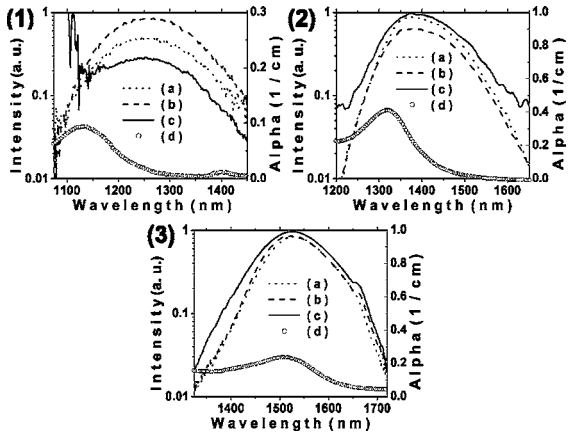

Fig. 7. Luminescence from K^+–Na^+ ion-exchange waveguides in PbS QD-doped glasses with QD-absorption spectra shown in Fig. 1 with QD sizes of (1) $R=2.2$ nm, (2) $R=2.7$ nm, and (3) $R=3.2$ nm. In each of these figures, we show the bulk-glass PL spectra (a) before and (b) after K^+–Na^+ ion exchange. The luminescence collected from a waveguide is shown in spectrum (c) along with spectrum (d), the QD absorption for comparison. The pump wavelength was 1064 nm.

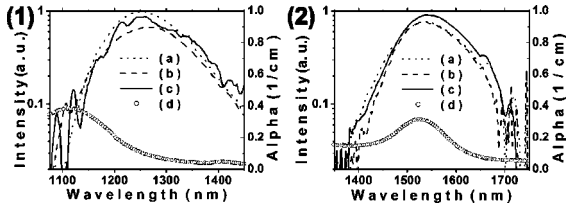

Fig. 8. Luminescence from Ag-film ion-exchange waveguides in PbS QD-doped glasses with QD-absorption spectra shown in Fig. 1 with QD sizes of (1) $R=2.2$ nm and (2) $R=3.2$ nm. In both these figures, we show the bulk-glass PL spectra (a) before and (b) after Ag-film ion exchange. The luminescence collected from a waveguide is shown in spectrum (c) along with spectrum (d), the QD absorption for comparison. The pump wavelength was 1064 nm.

Figure 7 shows luminescence from PbS QD-doped glasses that underwent K^+–Na^+ ion exchange. These PbS QD-doped glasses have the QD-absorption spectra shown in Fig. 1 with QD sizes of (1) $R=2.2$ nm, (2) $R=2.7$ nm, and (3) $R=3.2$ nm. Figure 8 shows luminescence from PbS QD-doped glasses that underwent Ag-film ion exchange. These PbS QD-doped glasses have the QD-absorption spectra shown in Fig. 1 with QD sizes of (1) $R=2.2$ nm and (2) $R=3.2$ nm. In Figs. 7 and 8, we show luminescence before and after ion exchange (bulk) and collected from an ion-exchanged waveguide. For the bulk measurements, labeled (a) and (b) in each figure, the 1064 nm pump beam was p polarized and set to Brewster's angle. The luminescence was collected in reflection at normal incidence by an $f/1$ lens and coupled into a spectrometer. For the waveguide luminescence measurements, we used a 0.4 NA microscope objective to couple the 1064 nm

pump beam into the waveguide. Here, the spectra labeled (c) was collected using the multimode fiber as depicted in Fig. 6(b).

There are some important features in these QD-luminescence spectra that we will point out. First, notice that these QD show a large Stokes shift between the linear absorption and the emission spectra. Also notice that this Stokes shift is largest and the PL spectrum is broadest for the QD-doped glass with ground-state resonance around 1100 nm and that the Stokes shift is smallest and the PL spectrum is narrowest for the QD-doped glass with ground-state resonance around 1500 nm. The difference in Stokes shifts can be explained by the level of quantum confinement of the QDs.[33] The Stokes shift is directly proportional to the quantum confinement. The QD-doped glass with ground-state resonance around 1100 nm has QDs with the highest level of quantum confinement and thus the largest Stokes shift. The QD-doped glass with ground-state resonance around 1500 nm has QDs with the lowest level of quantum confinement and thus the smallest Stokes shift. The difference of the spectral widths can be explained by the existence of trapped surface states in the QDs.[33] Since the QDs with ground-state resonance around 1100 nm are the smallest, they have the largest surface area per volume of the three samples. This large surface area per volume makes surface states more predominate and the binding energy of these trapped surface states larger. This makes the PL spectrum much broader than the underlying QD-absorption spectrum. Since the other samples have smaller QDs, this effect is reduced, making the PL spectra narrower.

Concerning the waveguide spectra, notice that, in all cases, there are no noticeable differences between the corresponding spectra, which demonstrates that the optical properties of the QDs remain unchanged through the ion-exchange process. Additionally, we found that the maximum luminescence signal occurred when the input and output optics were aligned to the waveguide. This confirms that the waveguides are doped with QDs. We emphasize that the waveguide luminescence collected using the three different collection schemes (see Fig. 6) had no significant differences.

4. CONCLUSIONS

In our case, the scattering dominates the waveguide propagation loss, so the underlying QD absorption and Rayleigh scattering cannot be seen. Phenomenologically, the better the surface quality or the less the surface interaction, the lower the exponent in the wavelength dependence of absorption. This was confirmed qualitatively by correlating the surface quality and homogeneity of all of our samples (four samples for each silver and potassium ion exchange) with the wavelength dependence. Additionally, we found that, in the Ag-film ion-exchanged samples, annealing decreased the waveguide propagation and coupling losses and the exponent of the wavelength dependence. Annealing spreads the index change and owing to the surface (boundary condition), this moves the mode further into the glass, reducing the surface interaction. Fully burying the waveguide would minimize the surface interaction. In fact, extremely low-loss surface waveguides have been produced in commercial ion-exchange glasses (IOG-10 and Corning 0211). Here, we find that the difficulty in adequate surface polishing is the current limitation. The other limiting factor was the lack of overall sample homogeneity. Therefore, for future investigations of waveguides in QD-doped glasses, the vital focus must be in improving the sample quality and polishing. Additionally, work must be done in the effort of successfully burying the waveguides in order to minimize the surface interaction.

In addition to fabricating waveguides in the host glass (no QDs), we produced waveguides in glasses with optical resonances at 1100, 1250, and 1550 nm by using both Ag-film and K^+-Na^+ ion exchange. Additionally, we confirmed that waveguides are doped with QDs by measuring their PL spectra. In addition to glass doped with PbS QDs, we were also able to produce K^+-Na^+ ion-exchanged waveguides in PbSe QD-doped glass. This demonstrates that these techniques are versatile and may be useful for fabricating waveguides in other semiconductor-doped glasses. This method may allow for the commercialization of manufacturing integrated optical circuits in semiconductor-doped glasses.

ACKNOWLEDGMENTS

Corning, Inc., prepared the QD-doped glasses and Kim Winick and Guangyu Li at the University of Michigan performed the RNF measurements. The authors thank S. Yliniemi and B. R. West for fruitful discussions. Support from the Technology and Research Incentive Fund (State of Arizona Photonics Initiative) and Center for Optoelectronic Devices, Interconnects, and Packaging is appreciated.

J. M. Auxier and N. F. Borrelli can be reached by e-mail at auxier@optics.arizona.edu and BorrelliNF@corning.com.

REFERENCES

1. J. M. Auxier, M. M. Morrell, B. R. West, S. Honkanen, A. Schülzgen, S. Sen, N. F. Borrelli, and N. Peyghambarian, "Ion-exchanged waveguides in glass doped with PbS quantum dots," Appl. Phys. Lett. **85**, 6098–6100 (2004).
2. J. M. Auxier, S. Honkanen, M. M. Morrell, M. A. Leigh, S. Sen, N. F. Borrelli, and A. Schülzgen, "Small mode-size waveguides in quantum-dot-doped glasses by Ag-film ion exchange," J. Appl. Phys., to be published.
3. N. F. Borrelli and D. W. Smith, "Quantum confinement of PbS microcrystals in glass," J. Non-Cryst. Solids **180**, 25–31 (1994).
4. Al. L. Éfros and A. L. Éfros, "Interband absorption of light in a semiconductor sphere," Sov. Phys. Semicond. **16**, 772–775 (1982).
5. Y. Wang, A. Suna, W. Mahler, and R. Kasowski, "PbS in polymers. From molecules to bulk solids," J. Chem. Phys. **87**, 7315–7322 (1987).
6. I. Kang and F. W. Wise, "Electronic structure and optical properties of PbS and PbSe quantum dots," J. Opt. Soc. Am. B **14**, 1632–1646 (1997).
7. E. Hanamura, "Very large optical nonlinearity of semiconductor microcrystallites," Phys. Rev. B **37**, 1273–1279 (1988).
8. K. Wundke, S. Pötting, J. M. Auxier, A. Schülzgen, N. Peyghambarian, and N. F. Borrelli, "PbS quantum-dot-doped glasses for ultrashort-pulse generation," Appl. Phys.

Lett. **76**, 10–12 (2000).
9. A. M. Malyarevich, I. A. Denisov, V. G. Savitsky, K. V. Yumashev, and A. A. Lipovskii, "Glass doped with PbS quantum dots for passive Q switching of a 1.5-μm laser," Appl. Opt. **39**, 4345–4347 (2000).
10. K. Wundke, J. M. Auxier, A. Schülzgen, N. Peyghambarian, and N. F. Borrelli, "Room-temperature gain at 1.3 μm in PbS-doped glasses," Appl. Phys. Lett. **75**, 3060–3062 (1999).
11. T. J. Cullen, C. N. Ironside, C. T. Seaton, and G. I. Stegeman, "Semiconductor-doped glass ion-exchanged waveguides," Appl. Phys. Lett. **49**, 1403–1405 (1986).
12. P. T. Guerreiro, S. G. Lee, A. S. Rodrigues, Y. Z. Hu, E. M. Wright, S. I. Najafi, J. Mackenzie, and N. Peyghambarian, "Femtosecond pulse propagation near a two-photon transition in a semiconductor quantum-dot waveguide," Opt. Lett. **21**, 659–661 (1996).
13. B. R. West, P. Madasamy, N. Peyghambarian, and S. Honkanen, "Modeling of ion-exchanged glass waveguide structures," J. Non-Cryst. Solids **347**, 18–26 (2004).
14. A. Tervonen, "A general model for fabrication processes of channel waveguides by ion exchange," J. Appl. Phys. **67**, 2746–2752 (1990).
15. J. Albert and J. W. Y. Lit, "Full modeling of field-assisted ion exchange for graded index buried channel optical waveguides," Appl. Opt. **29**, 2798–2804 (1990).
16. N. F. Borrelli, *Microoptics Technology: Fabrication and Applications of Lens Arrays and Devices* (Marcel Dekker, 1999).
17. S. I. Najafi, *Introduction to Glass Integrated Optics* (Artech House, 1992).
18. K. S. Chiang, "Construction of refractive-index profiles of planar dielectric waveguides from the distribution of effective indexes," J. Lightwave Technol. **LT-3**, 385–391 (1985).
19. J. Viljanen and M. Leppihalme, "Fabrication of optical strip waveguides with nearly circular cross section by silver ion migration technique," J. Appl. Phys. **51**, 3563–3565 (1980).
20. S. Honkanen, A. Tervonen, H. von Bagh, and M. Leppihalme, "Ion exchange process for fabrication of waveguide couplers for fiber optic sensor applications," J. Appl. Phys. **61**, 52–56 (1987).
21. S. Yliniemi, B. R. West, and S. Honkanen, "Ion-exchanged glass waveguides with low birefringence for a broad range of waveguide widths," Appl. Opt. **44**, 3358–3363 (2005).
22. S. Honkanen, A. Tervonen, H. von Bagh, A. Salin, and M. Leppihalme, "Fabrication of ion-exchanged channel waveguides directly into integrated circuit mask plates," Appl. Phys. Lett. **51**, 296–298 (1987).
23. P. Madasamy, S. Honkanen, D. F. Geraghty, and N. Peyghambarian, "Single-mode tapered waveguide laser in Er-doped glass with multimode-diode pumping," Appl. Phys. Lett. **82**, 1332–1334 (2003).
24. P. Polyhonen, S. Honkanen, A. Tervonen, and M. Tahkokorpi, "Planar 1/8 splitter in glass by photoresist masked silver film ion exchange," Electron. Lett. **27**, 1319–1320 (1991).
25. R. Göring and M. Rothhardt, "Application of the refracted near-field technique to multimode planar and channel waveguides in glass," J. Opt. Commun. **7**, 82–85 (1986).
26. K. I. White, "Practical application of the refracted near-field technique for the measurement of optical fibre refractive index profiles," Opt. Quantum Electron. **11**, 185–196 (1979).
27. C. A. Hill and D. R. Hall, "Coupling loss theory of single-mode waveguide resonators," Appl. Opt. **24**, 1283–1290 (1985).
28. D. Marcuse, "Mode conversion caused by surface imperfections of a dielectric slab waveguide," Bell Syst. Tech. J. **48**, 3187–3215 (1969).
29. D. J. Walter and J. Houghton, "Attenuation in thin film optical waveguides due to roughness-induced mode coupling," Thin Solid Films **52**, 461–476 (1978).
30. D. Marcuse, *Light Transmission Optics*, 2nd ed. (Van Nostrand Reinhold, 1982).
31. A. W. Snyder and J. D. Love, *Optical Waveguide Theory* (Chapman and Hall, 1983).
32. A. N. Sloper and M. T. Flanagan, "Scattering in planar surface waveguide immunosensors," Sens. Actuators B **11**, 537–542 (1993).
33. J. M. Auxier, K. Wundke, A. Schülzgen, N. Peyghambarian, and N. F. Borrelli, "Luminescence and gain around 1.3 μm in PbS quantum dots," in *Conference on Lasers and Electro-Optics (CLEO)*, Postconference Digest, Vol. 39 of OSA Trends in Optics and Photonics (Optical Society of America, 2000), pp. 385–386.